The effect of wave-induced turbulence on intertidal mudflats: Impact of boat traffic and wind

R. Verney, Julien Deloffre, J.C. Brun-Cottan, R. Lafite

Continental Shelf Research
Volume 27, Issue 5, 1 March 2007, Pages 594-612
http://dx.doi.org/10.1016/j.csr.2006.10.005

The effect of wave-induced turbulence on intertidal mudflats: Impact of boat traffic and wind

R. Verney[a,b], J. Deloffre[b], J.-C. Brun-Cottan[c] and R. Lafite[b]

[a] IFREMER, BP70, 29280 Plouzane, France
[b] UMR CNRS 6143 M2C, University of Rouen, 76821 Mont Saint Aignan Cedex, France
[c] UMR CNRS 6143 M2C, University of Caen, 24 Allée des Tilleuls, 14000 Caen, France

*: Corresponding author : romaric.verney@ifremer.fr

Abstract:

Semi-diurnal and fortnightly surveys were carried out to quantify the effects of wind- and navigation-induced high-energy events on bed sediments above intertidal mudflats. The mudflats are located in the upper fluvial part (Oissel mudflat) and at the mouth (Vasière Nord mudflat) of the macrotidal Seine estuary. Instantaneous flow velocities and mudflat bed elevation were measured at a high frequency and high resolution with an acoustic doppler velocimeter (ADV) and an ALTUS altimeter, respectively. Suspended particulate matter concentrations were estimated by calibrating the ADV acoustic backscattered intensity with bed sediments collected at the study sites. Turbulent bed shear stress values were estimated by the turbulent kinetic energy method, using velocity variances filtered from the wave contribution. Wave shear stress and maximum wave–current shear stress values were calculated with the wave–current interaction (WCI) model, which is based on the bed roughness length, wave orbital velocities and the wave period (T_S). In the fluvial part of the estuary, boat passages occurred unevenly during the surveys and were characterized by long waves (T_S>50 s) induced by the drawdown effect and by short boat-waves (T_S<10 s). Boat waves generated large bottom shear stress values of 0.5 N m^{-2} for 2–5 min periods and, in burst of several seconds, larger bottom shear stress values up to 1 N m^{-2}. At the mouth of the estuary, west south-west wind events generated short waves (T_S<10 s) of H_S values ranging from 0.1 to 0.3 m. In shallow-water environment (water depth <1.5 m), these waves produced bottom shear stress values between 1 and 2 N m^{-2}. Wave–current shear stress values are one order of magnitude larger than the current-induced shear stress and indicate that navigation and wind are the dominant hydrodynamic forcing parameters above the two mudflats. Bed elevation and SPM concentration time series showed that these high energy events induced erosion processes of up to several centimetres. Critical erosion shear stress (τ_{ce}) values were determined from the SPM concentration and bed elevation measurements. Rough τ_{ce} values were found above 0.2 N m^{-2} for the Oissel mudflat and about 1 N m^{-2} for the Vasière Nord mudflat.

These results demonstrate the advantages of combining the measurement of instantaneous velocity and bed elevation to determine in situ the erosion and deposition processes as a function of bottom shear stress variations.

Keywords: Wind waves; Boat waves; Bottom shear stress; Bed roughness length; Bed erosion; Intertidal mudflat; Seine Estuary

Nomenclature

A (m) : Semi-orbital excursion

C_{TKE}: Best fit coefficient for K-τ_{TKE} conversion

C_{SPM} (mg l^{-1}): Suspended particulate matter concentration

f (Hz) : Frequency

f_{NL}: Correction coefficient for non linear interaction between wave and current

f_W: Wave friction factor

H_S (m): Significant wave height

H_{RMS} (m): Root-mean-square wave height

h (m): Water height

k: Wave number

K (m^2 s^{-2}): Turbulent kinetic energy

kp (km): Kilometric point, distance from Paris (kp 0 : Pont Marie)

SNR (dB): ADV signal to noise ratio

T_S (s): Significant wave period

u,v,w (m s^{-1}): Instantaneous current velocity components following the coordinates East, North ,Up

$\overline{U},\overline{V},\overline{W}$ (m s^{-1}): Average current velocity components

u', v', w' (m s^{-1}): Fluctuating current velocity components

u_t', v_t', w_t' (m s^{-1}): turbulent component of the instantaneous velocity

u_W', v_W', w_W' (m s^{-1}): Orbital velocity component of the instantaneous velocity

U(z) (m s^{-1}): Mean horizontal current velocity

U_W (m s^{-1}): Maximum orbital velocity

u* (m s^{-1}): Friction velocity

z (m): ADV recording height above the bed

z_0 (m): Bed roughness length

Greek letters

κ: Von Karman constant

λ: ADV acoustic wave length

ρ (kg m^{-3}): Water density

ρ_b (kg m^{-3}): Sediment bulk density

τ_{ce} (N m^{-2}): Critical erosion shear stress

τ_{TKE} (N m^{-2}): Turbulent kinetic energy shear stress

τ_W (N m^{-2}): Maximum wave shear stress

τ_m (N m^{-2}): Mean bed shear stress integrating non linear wave-current interactions

τ_{WC} (N m^{-2}): Maximum wave-current shear stress

$\tau_{W\text{-}SW}$ (N m^{-2}): Wave shear stress for short-period boat-induced waves

$\tau_{W\text{-}LW}$ (N m^{-2}): Wave shear stress for long-period boat-induced waves

$\tau_{W\text{-}SW+LW}$ (N m^{-2}): Wave shear stress for boat-induced long waves and short waves

τ_C (N m^{-2}) : Current shear stress

ν (m^2 s^{-1}): Kinematic viscosity of water

1. Introduction

Estuarine intertidal mudflats, which store fine-grained sediment, represent key areas for the investigation of sediment transport dynamics and estuarine water quality management. When suspended particulate matter (SPM) settles, contaminants associated with it are deposited on estuarine intertidal mudflats, which thus become the main areas of contaminants accumulation. Previous studies have demonstrated that intertidal mudflats are subjected to successive periods of erosion and sedimentation which are controlled by sediment supply and hydrodynamic forcing parameters such as tides, fluvial discharge and wind (Dyer, 1994; Allen and Duffy, 1998; Uncles et al., 1998; O'Brien et al., 2000). Therefore, the storage of fine sediment by intertidal mudflats may be temporary, as the mudflats are subjected to erosion events of variable intensity and duration, from one millimetre per day to several centimetres in a few minutes (Deloffre et al., 2005). When a major erosion event occurs, the large amount of reworked sediments and the particle-associated contaminants released into the water column increase the risk of localized pollution (Cundy et al., 2005), especially during periods when fluvial discharge is low and there therefore is little dilution.

Erosion and resuspension processes occur when the bottom shear stress exceeds a critical threshold value (Mitchener and Torfs, 1996; Black and Paterson, 1997). Extending our knowledge of the erosion processes requires both accurate measurements of the hydrodynamic features near the bottom and a good estimation of the properties of the surface sediment. Recent improvements in acoustic devices allow accurate high frequency and 3D current velocity measurements and thus provide reliable and consistent shear stress measurements (Kawanisi and Yokosi, 1997; Voulgaris and Trowbridge, 1998; Talke and Stacey, 2003; Voulgaris and Meyers, 2004). A recent study carried out in the macrotidal Seine estuary focused on the tidal-induced bottom shear stress variability (Verney et al., 2006): the results demonstrated that tidal-induced shear stress measured at different location in the macrotidal Seine estuary exceeded the calculated erosion threshold only during short high energy events (HEEs). In estuarine areas, HEEs may be caused by waves generated by boat traffic and wind, which increase the bottom shear stress (Grant and Madsen, 1979; Soulsby et al., 1993; Parchure et al., 2001).

The objective of this study is to focus on the HEEs observed on several intertidal mudflats in a macrotidal estuary to identify and quantify the hydrodynamic factors causing the events, and to investigate the impacts of HEEs on the mudflat dynamics. This study introduces a new approach for determining the relationship between hydrodynamic parameters and mudflat erosion processes: the coupling of accurate near-bed hydrodynamic measurements with bed elevation measurements.

2. Field site

Before reaching the turbidity maximum zone, the SPM entering into the macrotidal Seine estuary is temporarily trapped in several fine-sediment storage areas sheltered from the strongest tidal-induced hydrodynamics conditions (Fig. 1) (Guezennec et al., 1999; Lesourd et al., 2003; Deloffre et al., 2005). Hydrodynamic conditions in the Seine Estuary are controlled by the semi-diurnal tidal cycle and are modulated seasonally by fluvial discharge (Guezennec et al., 1999). During the highest spring tides, the tidal range at the mouth of the estuary (kp 360) is up to 7 m and decreases upstream to 2 m at the upper limit of the estuary (kp 202). During periods of low fluvial discharge, the estuary is divided into two hydrodynamic compartments: a flood-dominated compartment downstream from kp 300 (Le Trait) and an ebb-dominated compartment upstream from kp 300 (Verney et al., 2006). The influence of wind on hydrodynamic features, i.e. wind waves and swell, is observed only at the estuary mouth when the wind is from the west-south-west (Le Hir et al., 2000; Silva Jacinto, 2002).

Over the last century, the regional authorities have put an emphasis on facilitating economic exchanges and in particular on encouraging sea-vessel traffic in the Seine estuary from its mouth to the Port of Rouen (kp 245) (Lafite and Romana, 2001; Lesourd et al., 2001). This has resulted in the construction of embankments and in heavy dredging activities to keep the main navigation channel operational for sea vessels downstream from Rouen. Boat traffic within the Seine estuary is divided in two sectors: upstream from Rouen the traffic consists exclusively of barges, which transport 3.5Mt annually, whereas downstream from Rouen both barges and sea-going vessels travel the estuary, with

145 more than 3,400 sea-vessels sailing seaward (Data from the Port Authorities of Rouen). Such a high
146 amount of boat traffic has the potential to contribute to local changes in hydrodynamic conditions.
147
148 For this study, two sites, representing the fluvial and marine parts of the estuary, were investigated: the
149 Oissel mudflat (kp 230) and the Vasière Nord mudflat (kp 355) (Fig 1). The sites were chosen on the
150 basis of recent work on the Seine estuary (Guezennec et al., 1999; Lesourd et al., 2003; Deloffre et al.,
151 2005; Deloffre et al., In press; Verney et al., 2006). The Oissel mudflat is one of the largest intertidal
152 storage areas of fine sediment in the fluvial part of the estuary, with a surface area of 9500 m^2. A two-
153 year high frequency survey of the bed elevation indicates that muddy sediments settle during high
154 river flow, with deposition rates up to 7.5 mm d^{-1}, and net deposits of 5 to 8.5 cm per episode
155 depending on the flux of suspended solids discharging at Poses (the upstream limit of the estuary). The
156 bed sediments are a mixture of sand and mud, and are characterised by modes of 20 and 200 µm
157 (Deloffre et al., 2005). During periods of low discharge, the previously-deposited material is eroded
158 continuously at the rate of 0.75 mm d^{-1} and transported downstream. However, significant erosion
159 events of several centimetres are occasionally observed. Hydrodynamic surveys during periods of low
160 discharge have demonstrated that low tidal-induced bottom shear stress is lower than 0.2 N m^{-2} and
161 thus not sufficient to explain the large erosion events, yet several HEEs that generated bottom shear
162 stress larger than 1 N m^{-2} were observed (Verney et al., 2006).
163
164 The Vasière Nord mudflat, the largest mudflat in the estuary (3.2 km^2, (Lesourd et al., 2003)), and is
165 located in the northern part of the estuary mouth. Here, unlike the Oissel mudflat, the annual high
166 frequency survey shows that deposition occurs in bursts during periods of low fluvial discharge, and is
167 closely related to the highest spring tides and the presence of the turbidity maximum zone in the
168 estuary mouth (Deloffre et al., In press). These deposits are dominated by fine sediments (<50 µm),
169 which represent 70 to 90 % of the material (Lesourd, 2000). As in the upstream fluvial mudflat, HHEs
170 of several centimetres are observed, mostly after deposition. ADV current velocity measurements in
171 spring and neap tide conditions have revealed low tidal-induced bottom shear stress values, except
172 during the rising flood period of the highest spring tides (Verney et al., 2006). The sampling station

above the Vasière Nord mudflat is located at mid-cross-section and 6.6 m above the reference sea level.

3. Materials and methods

In order to accurately identify HEEs, sedimentary and hydrodynamic parameters were monitored with high frequency devices over tidal cycles. In addition, fortnightly cycle surveys were carried out to investigate the mudflat response to HEEs. All surveys were carried out during periods of low fluvial discharge.

3.1. Bed-elevation measurements: the ALTUS altimeter

The ALTUS altimeter is an autonomous 2 MHz acoustic transducer coupled with a pressure sensor (Bassoullet et al., 2000). This device allows long term monitoring (Deloffre et al., 2005; Deloffre et al., In press), but is also suitable for high-frequency surveys (sampling frequency up to 1 Hz) with a data storage capacity of several weeks. The ALTUS provides bed elevation and water level measurements with resolution of 0.2 mm and 20 mm respectively. For this study, the transducer was positioned 20 cm above the bed, with a sampling frequency of one measurement every three minutes.

3.2. Hydrodynamic characteristics: ADV measurements

Stations were instrumented with a 6 MHz Nortek Vector Acoustic Doppler Velocimeter during periods of low fluvial discharge (<400 m^3 s^{-1}). The apparatus was fixed on a rigid aluminium frame, which was directed perpendicular to the main channel axis to minimize frame-induced noise. This set-up has been found to be particularly suitable for turbulent intensity determinations (Kawanisi and Yokosi, 1997; Talke and Stacey, 2003; Voulgaris and Meyers, 2004). ADV measurements give access to the three directional components of the current velocity, 7 cm above the bed, and to the water level variations, with a pressure sensor located 45 cm above the bed. Velocity measurements were recorded

in the East/North/Up coordinates, automatically compensating for any movement of the instrument using data provided by the ADV internal compass. This minimizes errors due to ADV misalignment with the vertical. For each tidal survey, the ADV ran continuously at the sampling frequency of 32 Hz. For semi-lunar surveys, the ADV collected measurements at 2 Hz for 180 s bursts, every 13 min. Mean current velocity and bottom shear stress were obtained by averaging instantaneous and fluctuating components of the flow over the burst duration.

3.2.1. Calculation of the bottom shear stress

Various methods are presented in the literature for the calculation of bottom shear stress values from measured instantaneous current velocities : the Logarithmic velocity Profile (LP) method (Fugate and Friedrichs, 2002; Simpson et al., 2005), the Turbulent Kinetic Energy (TKE) method (Soulsby, 1983; Williams et al., 1999; Talke and Stacey, 2003), the covariance (COV) method (Kim et al., 2000; Voulgaris and Meyers, 2004) and the Inertial Dissipation (ID) method (Huntley, 1988; Kim et al., 2000; Trembanis et al., 2004). The operational limitations for applying these methods in estuarine environments have been discussed by various authors (Soulsby et al., 1993; Kim et al., 2000; Hutnance et al., 2002). HEEs observed in the Seine estuary (Verney et al., 2006) are assumed to be induced by wave events. Therefore, neither the LP nor the COV methods can be used, as the LP method is based on time-averaged flow velocity and the COV method cannot separate tidal- and wave-induced fluctuations.

The method best suited to the investigation of wave-current shear interactions is the TKE method, as a spectral analysis of the instantaneous velocity provides both turbulent and wave characteristics (Soulsby and Humphery, 1990). This method is based on the separation of the wave-induced (u'_w, v'_w, w'_w) and turbulence-induced (u'_t, v'_t, w'_t) variances of each fluctuating velocity components u', v' and w'. During wave events, the energy spectrum consists of the superposition of the conventional turbulent spectrum featured by the Kolmogorov -5/3 roll off in the inertial subrange and a typical wave spectrum, identified as a peak of energy in the wave frequency range (typically between 1 and 0.1Hz

for wind waves). According to Soulsby and Humphery (1990), the energy spectrum is split in two parts at the base of the wave peak. This method is performed automatically on the full u, v and w dataset where, according to the Kolmogorov theory, the separation line corresponds to an interpolation of the -5/3 slope (in log space), with a reference point at f =0.1Hz (outside the wave frequency range). The area below the interpolation line therefore corresponds to the turbulent kinetic energy of the velocity component considered (respectively u'^2, v'^2 or w'^2), and the area above the line to the wave variance contained in the fluctuating part of the velocity component.

The TKE shear stress (τ_{TKE}) is determined from the turbulent kinetic energy K:

$$\tau_{TKE} = \rho C_{TKE} K = 0.5 \rho C_{TKE} \left(\overline{u_t'^2} + \overline{v_t'^2} + \overline{w_t'^2} \right) \quad (4)$$

Various C_{TKE} values are proposed in the literature for different estuaries, ranging from 0.18 to 0.21 (Soulsby, 1983; Kim et al., 2000; Talke and Stacey, 2003). For the Seine estuary, Verney et al. (2006) found C_{TKE}=0.19 to be the best-fit constant for the tidal-induced shear stress on intertidal mudflats. τ_{TKE} is the best estimation of the bottom shear stress attributable to current in the presence of waves (Williams et al., 1999).

3.2.2. Wave shear stress

The significant wave height (H_S), root-mean-square wave height (H_{RMS}) and significant wave period (T_S) are calculated from the water level (h) time series over a 1 min burst. Significant wave orbital velocity U_W is calculated from the wave variances (u_W' ans v_W') deduced from the turbulent spectrum analysis, such as (Myrhaug et al., 1998):

$$Uw = 2 * \sqrt{u_w'^2 + v_w'^2} \quad (5)$$

The wave shear stress τ_W is given by:

$$\tau_W = 1/2 * \rho * f_W * U_W^2 \quad (6)$$

where f_W is the wave friction factor, which depends on the turbulent characteristics of the flow. In this study flow is turbulent, and the friction factor is obtained from the relation (Soulsby, 1997):

$$f_W=1.39*(A/z_0)^{-0.52} \quad (7)$$

where A is the semi-orbital excursion : $A=U_W T_S/2\pi$ and z_0 is the bed roughness length.

3.2.3. Wave-current shear stress

Waves and current both contribute to the bottom shear stress; various models have been developed to determine the combined wave-current shear stress (Grant and Madsen, 1979; Fredsoe, 1984). The method used in this study refers to the parametric Wave-Current Interaction (WCI) model proposed by Soulsby (1995). The equations used are based on theories previously developed and fitted to field and tank experiments. Soulsby introduced a correction coefficient f_{NL} that takes into account the non-linear interaction between the waves and the current in the mean bed shear stress:

$$f_{NL}=1.2*(\tau_w/(\tau_w+\tau_C))^{3.2} \quad (8)$$

The mean bed shear stress τ_m is:

$$\tau_m=\tau_C\,(1+f_{NL}) \quad (9)$$

In the present study, wave-current interaction is incorporated into the τ_{TKE} calculations, and therefore τ_m is equal to τ_{TKE}. Given that Ψ is the angle between the waves and the current, the total wave-current bed shear stress becomes:

$$\tau_{WC} = \sqrt{\left(\tau_{TKE} + \tau_W * \cos(\Psi)\right)^2 + \left(\tau_W * \sin(\Psi)\right)^2} \quad (10)$$

3.3. Bed roughness calculation

Bed roughness length is a key parameter that must be determined when calculating wave shear stress. At the tidal scale, however, bed roughness length varies rapidly, as it is a function of sediment grain-size distribution, bedforms present, and suspended sediment concentration (Collins et al., 1998; Trembanis et al., 2004; Voulgaris and Meyers, 2004). Moreover, in the presence of waves, the bed roughness length is greatly affected by the increase in eddy viscosity within the wave boundary layer (Grant and Madsen, 1979; Soulsby and Humphery, 1990) and no longer corresponds to the physical

bed roughness used in the WCI method to calculate wave-current shear stress. Therefore, the bed roughness length is calculated outside wave events from the drag coefficient $C_d(z)$ for each site at the tidal scale, and assuming the development of a logarithmic velocity profile (Soulsby and Humphery, 1990):

$$u*^2 = C_d(z) * U(z)^2 \quad (11)$$

$$\frac{U(z)}{u*} = \frac{1}{\kappa} \log\left(\frac{z}{z_0}\right) \quad (12)$$

where u* is the friction velocity calculated from τ_{TKE} such that:

$$u* = \sqrt{\frac{\tau_C}{\rho}} \quad (13)$$

and

$$z_0 = z * \exp\left(-\frac{\kappa}{\sqrt{C_d(z)}}\right) \quad (14)$$

3.4. SPM concentration: estimation from the ADV backscatter

In addition to current measurements, acoustic Doppler devices (ADCPs or ADVs) provide backscattered acoustic amplitudes and signal to noise ratios (SNR) for measurement validation. Calibrating the backscattered acoustic intensity with SPM concentrations is complex, but provides key information on sediment transport features, i.e. hydrodynamic and suspended sediment characteristics at high frequency (Kawanisi and Yokosi, 1997; Voulgaris and Meyers, 2004). The main difficulty is that the backscattered acoustic intensity depends on the SPM concentration, grain-size distribution and composition in the volume sampled. The optimal dynamical response of the ADV backscattered acoustic intensity is given for particle sizes D_{opt} where $D_{opt}*\lambda/2=1$ and λ is the ADV unity for coarser particles, assuming that the entire emitted signal is returned to the transducers. For a 6 MHz ADV such as the one used for this study, the operational size range is estimated to be between 10 µm and 200 µm, with the optimal size calculated to be 80 µm, similar to the mode value of the grain-size

distribution of the muddy material present in the estuary (Lesourd, 2000). This validates the use of the ADV backscatter as an appropriate proxy for estimating SPM concentration.

In parallel to physical acoustic theories (Thorne and Hanes, 2002), Voulgaris and Meyers (2004) proposed empirical calibrations to convert backscatter signal to SPM concentration. For this study, calibration experiments were carried out in the laboratory using surface sediments collected at the two sampling stations (Fig. 2). The calibration experiment is based on a classical calibration set-up, i.e., the ADV is immersed in a tank that is homogeneously filled step by step with surface sediments to increase the SPM concentration (C_{SPM}). The ADV acoustic backscattered intensity is recorded for 30 s and a water sample is collected to determine the weighted C_{SPM}. The burst-averaged SNR values are used to quantify the backscattered acoustic intensity, and then compared with the measured C_{SPM} in the tank for all sediments (Fig. 2). Log(SNR) is linearly correlated with $\log(C_{SPM})$ for both sites :

$$\log(C_{SPM})=-26.48+15.03*\log(SNR) \text{ (Fig. 2 – Vasière Nord [1])} \quad (R^2=0.84) \tag{15}$$

$$\log(C_{SPM})=-28.02+15.91*\log(SNR) \text{ (Fig. 2 – Oissel [2])} \quad (R^2=0.98) \tag{16}$$

For these two calibration sets, the operational concentration ranges from 10 to 5000 mg l^{-1}. At lower concentrations, the backscattered intensity is highly variable and the calibration curve does not show a consistent pattern. For C_{SPM} higher than 5000 mg l^{-1}, the ADV response no longer changes with increasing C_{SPM}. However, in practice this upper limit is never reached as C_{SPM} rarely exceeds 3000 mg l^{-1} in the Seine estuary (Lesourd, 2000; Deloffre et al., 2005).

This empirical method for ADV-SPM calibration was used by Voulgaris and Meyers (2004) (Fig. 2). However, it should be noted that these authors used a 10 MHz Sontek ADV that is more sensitive to finer particles and lower C_{SPM}. This explains the difference between their calibration equation and that presented here.

4. Results

4.1. High Energy Events and forcing parameters

4.1.1. The estuary mouth: the wind influence

A typical W-SW wind event occurred on May 5, 2004, with an average wind speed of 8 m s^{-1} and gusts of 10 m s^{-1} (Fig. 3). W-SW wind events of similar intensities are known to increase wave action in the estuary mouth (Silva Jacinto, 2002). The sampling station is located in the middle of the largest mudflat in the estuary, at the height of 6.6 m above reference sea level, thus water heights above the station rarely exceed 1 m during neap tide conditions. The water level fluctuations measured by the ADV and filtered from the tidal amplitude are shown in Fig. 3a. Waves are observed continuously during the tidal cycle, with significant wave periods varying from 3 to 8 s and significant wave heights ranging from 0.1 to 0.35 m (Fig. 3b). Waves were present continuously during this survey, so the bed roughness length was not calculated. Instead, the bed roughness calculated for the same site during the fortnightly cycle was used (z_0=0.37 mm) as well as the bed roughness lengths given by Soulsby (1997) for mud and muddy/sandy sediment (i.e., 0.2 and 0.7 mm respectively) to investigate the variability of the results.

The wave-current shear stress fluctuations are shown in Fig 3c and compared to the TKE shear stress. During the survey, τ_{WC} values were twice to one order of magnitude higher than τ_{TKE}, with characteristic values ranging from 0.6 to 4 N m^{-2} and 0.1 to 1 N m^{-2}, respectively, for τ_{WC} and τ_{TKE}. This confirms that wind-waves are the dominant forcing parameter at the estuary mouth. The largest waves (>0.2 m) are associated with τ_{WC} values above 1 N m^{-2}. Comparing τ_{WC} values obtained for the different bed roughness values (Fig. 3c – shadow area) demonstrates high sensitivity of the z_0 calculation: estimating τ_{WC} with z_0=0.2 mm or 0.7 mm results in discrepancies of up to 100% compared with τ_{WC} calculated with z_0=0.37mm.

4.1.2. The fluvial estuary: the influence of boat traffic

Representative water level recordings from the Oissel mudflat are shown in Fig. 4a. Examination of the water elevation time-series reveals the passage of at least five boats. These passages are identified by the boat-generated wave packets with amplitudes up to 0.16 m.

A ship passage is examined in detail in Fig. 4b and Fig. 4c; the figures show typical vessel-generated water-level and current-velocity variations. These boat-induced variations affect the local hydrodynamics and are characterised by one long wave followed by short wave packets as reported in previous studies (Schoellhamer, 1996; Fagerburg and Pratt, 1998; Parchure et al., 2001).

Long waves are caused by the drawdown effect, which is defined as an abrupt diminution of the water level caused by the displacement of the boat. The occurrence and amplitude of the drawdowns are controlled by the width of the channel, the local water depth and some boat-related features, such as the shape of the hull and the boat speed, e.g., the narrower the width, the larger the drawdown (Schoellhamer, 1996; Fagerburg and Pratt, 1998). Here, the drawdown shows a wave period of 50 s and an amplitude of 0.06 m. The wave is reflected several times by the river banks and its amplitude decays with time. The drawdown substantially affects the local current velocities, causing horizontal velocity variations of 0.2 m s^{-1} (Fig. 4 c). This type of long wave is observed before the arrival of short wave packets. In Fig. 4b, the boat-generated short waves have a period of 3 s, the first and largest wave height is 0.1 m and following wave heights decrease with time. Wave packets are observed several times as a result of reflections on embankments. The boat passage affects the mudflat for 2- to 5-min periods, and induces high flow velocity fluctuations: the largest fluctuation amplitude is 0.3 m s^{-1} and then decreases with time (Fig. 4 c).

Waves generated by barges or vessels contribute to the bottom shear stress. This contribution can be estimated using the WCI model detailed in section 3.2.3. The bed roughness length for the Oissel

mudflat was estimated by Verney et al. (2006) to be 0.3 mm, from the calculation of the drag coefficient obtained by comparing mean current velocity U and friction velocity u* in the absence of waves. Wave height measurements revealed that the boat-generated waves are mono- or sometimes bi-modal. As described in the previous section, the WCI model is applied for waves characterised by a single period and a single height. Short and long waves were examined separately to estimate the shear stress contribution of each type of wave and to determine the total boat-induced bottom shear stress.

Long and short waves were filtered by band-pass filters from the spectral analysis of the raw-water level signal, with long and short wave frequencies assumed to range from 0.002 Hz to 0.1 Hz, and 0.1 Hz to 1 Hz, respectively. Fig. 5 focuses on a typical time series corresponding to Fig. 4b and details the procedure applied to calculate τ_{WC}. Once extracted from the raw signal (Fig. 5 a, b and c), the long and short wave signals are processed to calculate their respective wave periods and significant wave heights. Long wave properties are calculated over a 1 min period. However, this calculation period is too long to represent accurately the rapidly fluctuating short waves, and so the significant wave heights, periods and orbital velocities for short waves were calculated over an 8 s burst period. Short wave heights decay rapidly from 0.1 to 0.02 m in a few minutes. Significant long-wave heights up to 0.06 m are observed and the perturbations induced last for approximately 5 min with slight wave height decay. Similar to short waves, long waves affect the turbulent spectrum in the low frequency range (i.e. $f<0.1$ Hz). In the absence of long waves, the energy spectrum shows a quasi-stationary behaviour in this frequency range, while in the presence of long waves it greatly increases. A second cut off therefore is applied to the low frequency regime ($f<0.1$ Hz) to calculate the wave variance associated with long waves, fixed to a constant variance calculated for $f=0.1$Hz. Wave shear stresses for long ($\tau_{W\text{-}LW}$) and short ($\tau_{W\text{-}SW}$) waves are calculated from the WCI model equations (Eq. 5 to 10) (Fig. 5 d). In this case, $\tau_{W\text{-}LW}$ presents a maximum value of 0.1 N m^{-2} as a result of the drawdown effect, and $\tau_{W\text{-}SW}$ increases when short waves arrive, with a maximum value of 1 N m^{-2}. Low amplitude short waves are observed during the drawdown period, generating a wave shear stress of 0.08 N m^{-2}, lower than the $\tau_{W\text{-}LW}$ value. $\tau_{W\text{-}SW}$ and $\tau_{W\text{-}LW}$ then are summed to obtain the overall wave shear stress $\tau_{W\text{-}LW+SW}$, which is used to calculate the overall wave-current shear stress (τ_{WC}), from equations 8 to 10

(Fig. 5e). τ_{TKE} is one order of magnitude lower than τ_{WC} and non-linear wave effects on τ_{TKE} are observed. This procedure is extended to the entire dataset (Fig. 6). During the tidal cycle, τ_{TKE} is well correlated with the current velocity (Fig. 6: from 03h00 to 06h00).

All boat passages generate bottom shear stress with τ_{WC} values above 0.1 N m^{-2} and up to 2 N m^{-2}. The boat traffic in the Seine estuary is dense, and occasionally boats must either follow each other closely or pass each other with very little clearance in the narrow channel. This results in longer duration HEEs, characterised by a succession of multiple wave packets, which can combine with each other and generate larger waves and thus greater bottom shear stress (Fig. 6 – from 00h40 to 01h20). In this case, the turbulent flow relaxes slightly and does not reach a steady state until more than 20 min after the last barge passage.

4.2. Impact of the HEEs on the dynamics of the intertidal mudflats of the Seine estuary

The factors controlling the variability of the bottom shear stress intensity are identified by tidal surveys as the tidal currents (Verney et al., 2006), the W-SW wind events (at the mouth of the Seine estuary), and the passage of boats and barges (in the fluvial part of the estuary). Based on these studies, surveys were carried out in the fluvial part of the estuary and at the mouth of the estuary to monitor hydrodynamic and sedimentary processes during a semi-lunar cycle. The objective of this work is to investigate the impact of HEEs on the mudflat dynamics, and in particular the erosion and resuspension processes affecting the surface sediment.

4.2.1. Wind impact on mudflat behaviour

The Vasière Nord survey was carried out in spring tide conditions, which are reported as being favourable for sediment accretion above the mudflat (Deloffre et al., In press). The variations of the

442 bed elevation of the Vasière Nord mudflat are compared to the time series of τ_{WC}, SPM concentration,
443 water surface elevation, and wind and wave conditions (Fig. 7).
444
445 Throughout the survey, the water level above the mudflat never exceeded 1.5 m (Fig. 7 a). Wind speed
446 above 10 m s^{-1} are observed unevenly; they generate wind waves with an average wave height of 0.15
447 m and wave periods ranging from 2 to 10 s. Waves are always observed above the mudflat and the
448 lowest wave heights are less than 0.1 m and correlated with wind speeds below 5 m s^{-1} (Fig. 7 b).
449 Periods of large amplitude waves, above 0.2 m, are observed in bursts.
450
451 The weakest wave event occurred during VN1, and this period there was chosen to calculate a z_0 value
452 (wave heights >0.1m excluded), and estimated to be 0.37 mm. The combination of low water heights
453 and large wave amplitudes induces strong bottom shear stresses. Periods of wind-wave heights above
454 0.15 m are reported as HEEs and correspond to bottom shear stress values higher than 0.5 N m^{-2} for
455 periods lasting from the hour to the tidal scale (Fig. 7 c and d). The largest HEE (VN2) is correlated
456 with a SW wind event of 13 m s^{-1}, generating wave heights up to 0.3 m and τ_{WC} of 2 N m^{-2}. Calm
457 periods are associated with bottom shear stress values below 0.5 N m^{-2}.
458
459 The Vasière Nord mudflat underwent several periods of sedimentation and resuspension/erosion (Fig.
460 7f). A typical sedimentation/resuspension pattern is observed, characterized by a new deposit during
461 the flood period: VN1: +10 mm, VN3: +3 mm; VN4: +5 mm. Deposition events are correlated with
462 the weakest hydrodynamic conditions, i.e. τ_{WC}<0.8 N m^{-2} and wave heights below 0.15 m.
463 Resuspension and erosion periods are observed during HEEs characterised by τ_{WC} values greater than
464 1 N m^{-2}, induced by wind-wave heights above 0.15 m. These HEEs partly or entirely remove the
465 previously deposited sediment (Fig. 7f): VN1: -2 mm; VN2: -7 mm; VN3: -5 mm; VN4: -2.5 mm,
466 VN5: -7 mm, VN6: -2 mm. This material is re-enters the water column, as demonstrated by the
467 monitoring of C_{SPM}: every resuspension or erosion event is correlated with high C_{SPM} values above 100
468 mg l^{-1}, and occasionally as high as to 1500 mg l^{-1} (Fig. 7e)

469

470 At the scale of the survey, the total amount of deposited sediments is removed, and the net budget of
471 the erosion/sedimentation periods shows is an erosion of the bed of 5 mm. This erosion was confirmed
472 by field observation at the end of the survey: the surface of the mudflat was rippled, made up of hard
473 sandy-mud, and hard-mud pebbles were scattered over the mudflat as a consequence of strong
474 hydrodynamic conditions and erosion at the edge of the mudflat.

475

476 **4.2.2. Boat impact on mudflat behaviour**

477

478 The results of the bed roughness length calculation during the survey are shown in Fig. 8. They reveal
479 a variability of 30% around a mean value of 0.1 mm, and maximum value of 0.3 mm. These calculated
480 z_0 values are used for τ_{WC} calculations. The behaviour of the Oissel mudflat during a semi-lunar cycle
481 is examined in Fig. 9 in response to the variations in the bottom shear stress and the local C_{SPM}. The
482 average tidal-induced shear stress (boat passages excluded) is low (less than 0.1 N m^{-2}), which is
483 explained by the weak tidal currents in the upper reach of the estuary (Verney et al., 2006). C_{SPM} is
484 low, ranging from 10 to 50 mg l^{-1} (Guezennec et al., 1999; Deloffre et al., 2005). These low
485 hydrodynamic conditions are favourable for sedimentation: the altimetric survey shows a constant
486 sedimentation rate of 0.2 mm per tide.

487

488 Short HEEs (τ_{WC}>0.5 N m^{-2}) are recorded only irregularly (OI1, OI3, OI5, OI7, OI10); and they are
489 associated with an increase in C_{SPM} above 200 mg l^{-1} (Fig. 9a, b and c). Among all the HEEs reported,
490 only one is correlated with a large and abrupt bed erosion (f 6 mm for OI10 - Fig 9d). This erosion
491 event is clearly correlated with a boat passage, as indicated by bottom shear stress values higher than
492 0.5 N m^{-2}. This event affected only a longshore line of the mudflat, where erosion is visible and
493 indicated by a change in the bed surface: near the bank, the bed is flat and soft, and near the river, the
494 bed is rough and scattered with muddy pebbles, typical of erosional events. All other HEEs observed
495 during the survey were associated with a C_{SPM} increase, but no net erosion was recorded by the

altimeter during this survey: because of the local effect of boat-induced waves, this could correspond to erosion of another part of the mudflat, where bed shear stress exceeds the critical shear stress.

5. Discussion

5.1. Processes of erosion: boat-induced waves

Field measurements showed that barge passages in a narrow channel change the local hydrodynamics by generating a drawdown and packets of waves, and sometimes causing sediment resuspension (Fig. 4; Fig. 5; Fig. 9; Table 1). The drawdown is a low frequency variation of the water level, and its amplitude was reported to vary from 0.05 to 0.1 m. Short waves are grouped in wave packets of wave height ranging from 0.05 to 0.15 m. Boat passages cause short duration HEEs, which never exceeded 10 min. These observations are in agreement with the results of the field surveys and laboratory experiments reported by Parchure et al. (2001). These authors classified waves and drawdown intensities by boat type. They concluded that large vessels generated large drawdowns but low short-wave heights, contrary to leisure boats, which travel faster and thus generate small drawdowns but large short-wave heights. They also reported that barges induced more resuspension, with C_{SPM} varying from 100 to 500 mg l^{-1} close to the bed. These concentrations are similar to those measured from the ADV backscattered intensity on the Oissel mudflat after barge passages. This might reflect the bed dislocation/liquefaction effect of the long waves, which would layer the first centimetres that could then be removed by short waves (De Wit and Kranenburg, 1997).

The water height time series indicate the passage of many boats. The most substantial events are reported in Table I, along with their principal hydrodynamic features. Relations between boat-induced flow variations, sediment resuspension, and bed erosion are difficult to establish, because they are related to various criteria such as water level, wave amplitude and frequency, bed form, and bed structure (Parchure et al., 2001). However, comparison of the local hydrodynamic variations and the response of the bed sediments shows that resuspension processes mainly occur during both high and

low frequency velocity fluctuations (Table I, Boats 1, 5, 7 and 10). Low frequency current fluctuations occasionally generated low intensity resuspension (Table I, Boats 2, 4, 6, 8 and 9). Moreover, the erosion event observed by the ALTUS occurred when the average water height was the lowest, at approximately 0.3 m, which suggests that water level is a critical parameter for erosion in the upper part of the estuary. Despite the low probability of such HEEs (as they require both boat passage and low water level), their amplitudes demonstrate that boat traffic plays an important role at the annual scale in mudflat dynamics and sediment fluxes in the upper estuary. This is confirmed by Deloffre et al. (2005), who reported three or four periods of abrupt erosion per year during a two-year survey above the Oissel Mudflat. These large erosion processes occurred after a period of deposition of several centimetres, when bed sediment bulk densities and critical erosion shear stress are the lowest.

This emphasizes the need for further examination of very shallow water processes. The influence of boat-induced waves as they break on the mudflat, when the turbulent intensity is at its highest, is of special interest.

5.2. Bed sediment erodibility and critical erosion shear stress

The turbulent threshold effect on mudflat sediment erosion processes has been researched extensively over the last 30 years. This threshold effect is especially relevant for mathematical modelling of sediment transport, which uses the critical erosion shear stress as a major controlling parameter (Sanford and Maa, 2001). Many instruments have been developed to estimate this threshold in field studies or in laboratory flumes (Mitchener and Torfs, 1996; Black and Paterson, 1997; Tolhurst et al., 2000). All these instruments are based on the same experimental protocol, i.e. the shear stress applied is controlled and increased stepwise, and the erosion threshold is reached when the operator observes that C_{SPM} shows a substantial increase or exceeds a fixed level of C_{SPM} or turbidity. Similar measurements of the critical erosion shear stress can be carried out in situ by comparing time series of bottom shear stress values to erosion criteria, i.e. C_{SPM} and bed height measured by ADV and ALTUS devices.

552 Those two methods are applied for the Oissel mudflat measurements. A comparison of C_{SPM} values
553 and τ_{WC} values (Fig. 9 and 10) shows that substantial resuspension occurred when τ_{WC} was above 0.2
554 N m^{-2}, except for OI1 where no concentration increase was observed. Based on bed elevation
555 measurements, bed erosion occurred abruptly and only once during the study, and was associated with
556 high τ_{WC} values (between 0.3 and 0.8 N m^{-2}). The bed sediments of the Oissel mudflat are sandy-mud
557 with a thin layer of newly deposited sediments, as observed by the altimetric survey (Fig. 9). The
558 critical shear stress value calculated from the relation provided by Mitchener and Torfs (1996) for
559 sandy-mud sediments is 0.6 N m^{-2}, which is in the range of the τ_{ce} value estimated. However, the
560 altimeter did not measure any variation of the bed elevation during these events. This could be either
561 because the erosion affected only the thin upper layer of fluid mud deposited at the surface, the erosion
562 thickness being smaller than the ALTUS vertical resolution, or more probably because erosion
563 occurred elsewhere on the mudflat. Unlike devices dedicated to erosion threshold determination that
564 work with a confined controlled volume of water, the C_{SPM} method used in situ to determine τ_{ce} is
565 subjected to variations in both the intensity of the hydrodynamic processes and in the bed sediment
566 properties. Therefore, an increase in C_{SPM} observed by the ADV may be the result of bed erosion away
567 from the sampling site and thus not measurable by the ALTUS altimeter, the resuspended sediment
568 being then advected through the ADV sampling volume as modelled and discussed by Brun-Cottan et
569 al. (2000).
570
571 Estimating critical erosion shear stress is more complex at the estuary mouth: this site is influenced by
572 the turbidity maximum zone, and so the background C_{SPM} is naturally highly variable, and ranges from
573 10 to 1000 mg l^{-1} (Lesourd et al., 2003; Deloffre et al., 2005). The C_{SPM} method therefore cannot be
574 applied to determine τ_{ce}, and only the altimetric measurements are used (Fig. 7). The results
575 demonstrate that deposition periods correspond to τ_{WC} values below a critical value of 0.8 N m^{-2}, and
576 the lower the τ_{WC}, the higher the deposition rate. Erosion processes take place for τ_{WC} values higher
577 than 1 N m^{-2}. The relation between erosion rate and bed sediment properties is clearly observed: all
578 erosion events that occur after a period of deposition have an erosion rate that ranges from 0.1 to 0.165

579 g m^{-2} s^{-1} (VN2 to VN5). During VN5 and VN6, the erosion rate decreased from 0.1 to 0.035 g m^{-2} s^{-1},
580 whereas the mean shear rate was similar during these two tides (1.5 N m^{-2}). During VN5, the bed
581 surface sediment had been newly deposited during the previous tides, and should be characterised by a
582 lower bulk density and a lower critical erosion shear stress. During this tide, all newly deposited
583 sediments were removed and the bed level reached was lower than at any time during the previous
584 four days. Therefore, bed sediments during VN6 had been subjected to consolidation processes for
585 several days and should feature higher bulk densities and higher critical erosion shear stress, which
586 would explain the lower erosion rate during VN6. The critical erosion shear stress value of 1 N m^{-2} is
587 in the upper range of the critical erosion shear stress measured by Mitchener and Torfs (1996) for
588 newly-deposited muddy bed sediments and which ranges from 0.1 to 1.5 N m^{-2}.
589
590 The differences between critical erosion shear stress values calculated in this study and the values
591 proposed in the literature may be the results of differences in the hydrodynamic processes observed.
592 Most of the knowledge of erosion and deposition processes of muddy sediments is based on studies
593 that taking into account only the current velocities (Tolhurst et al., 2000). In contrast, this study
594 examined the impact of wave-induced shear stress on mudflat dynamics. Currently, our understanding
595 of the interaction between wave-induced shear stress, muddy sediment erodibility, and bed sediment
596 properties is limited to field observations (Winterwerp and van Kesteren, 2004). Thus, further research
597 is required to provide a better understanding of current only, wave only and current-wave erosion
598 processes in relation to muddy bed sediment properties.
599
600 **6. Conclusions**
601
602 The combined use of high frequency and high resolution altimetric measurements and near bottom
603 sediment hydrodynamic measurements during both tidal and semi-lunar surveys identified and
604 quantified wind and boat passage events and their impact on mudflats. The tidal surveys allowed
605 continuous recording of the current velocity and water height fluctuations. These measurements
606 allowed quantification of the boat- and wind- induced wave contributions to the bottom shear stress.

607 Bed elevation, bottom shear stress, and suspended particulate matter concentration measurements
608 close to the bottom were used to determine critical erosion and deposition shear stresses.
609
610 The fluvial part of the Seine estuary is affected by boat traffic. Boat-induced waves show a bimodal
611 pattern, with long and short waves, and generate bottom shear stresses stronger than 0.5 N m^{-2} for a
612 few minutes with peaks up to 1 N m^{-2}. In most cases, boat passages generate sediment resuspension
613 when bottom shear stress values exceeded 0.2 N m^{-2}. Large erosion processes (erosion of more than a
614 5 mm thickness) are observed under specific conditions such as low water height (h<30 cm) and high
615 amplitude waves. Low amplitude erosion processes are observed at very shallow water depths at the
616 beginning of the flood tide and at the end of the ebb tide, which could be caused by tidal currents or
617 boat passages. These observations highlight the need for further research on the effect of both very
618 shallow water processes and emersion/immersion processes on sediment dynamics.
619
620 At the mouth of the Seine estuary (Vasière Nord Mudflat), W-SW wind events generate waves with a
621 significant wave height of 0.1 to 0.3 m for wind speeds ranging from 7 to 15 m s^{-1}. Wind waves induce
622 bottom shear stress values higher than 0.5 N m^{-2} and up to 2 N m^{-2}. These results confirm that W-SW
623 wind events are the predominant forcing parameter for mudflat dynamics at the estuary mouth. Critical
624 deposition shear stress is estimated to 0.8 N m^{-2} and critical erosion shear stress to be 1 N m^{-2}.

7. Acknowledgments

Funding for this study was provided partly by the European INTERREG III RIMEW program and the Seine Aval Program. Romaric Verney was funded through a grant provided by the Regional Council of Haute Normandie (France). We would like to thank Mrs Dilys Moscato and Mrs Barbara Malher for their helpful review and Michel Simon for his technical support on field. Two anonymous reviewers are thanked for their helpful comments and useful corrections that greatly improved this work.

8. References

Allen, J. R. L. and Duffy, M. J. (1998) Temporal and spatial depositional patterns in the Severn Estuary, southwestern Britain: intertidal studies at spring-neap and seasonal scales, 1991-1993. Marine Geology, 146 (1-4) 147-171

Bassoullet, P., Le Hir, P., Gouleau, D. and Robert, S. (2000) Sediment transport over an intertidal mudflat: field investigations and estimation of fluxes within the "Baie de Marennes-Oleron" (France). Continental Shelf Research, 20 (12-13) 1635-1653

Black, K. S. and Paterson, D. M. (1997) Measurement of the erosion potential of cohesive marine sediments: a review of current in situ technology. Journal of Marine Environmental Engineering, 4 43-83

Brun-Cottan, J.-C., Guillou, S. and Li, Z. H. (2000) Behaviour of a puff of resuspended sediment : a conceptual model. Marine Geology, 167 355-373

Collins, M. B., Ke, X. and Gao, S. (1998) Tidally-induced flow structure over intertidal flats. Estuarine, Coastal and Shelf Science, 46 233-250

Cundy, A. B., Hopkinson, L., Lafite, R., Spencer, K., Taylor, J. A., Ouddane, B., Heppell, C. M., Carey, P. J., Charman, R., Shell, D. and Ullyott, S. (2005) Heavy metal distribution and accumulation in two Spartina sp.-dominated macrotidal salt marshes from the Seine estuary (France) and the Medway estuary (UK). Applied Geochemistry, 20 1195-1208

De Wit, P. J. and Kranenburg, C. (1997) The wave-induced liquefaction of cohesive sediment beds. Estuarine, Coastal and Shelf Science, 45 261-271

661 Deloffre, J., Lafite, R., Lesueur, P., Lesourd, S., Verney, R. and Guezennec, L. (2005) Sedimentary
662 processes on an intertidal mudflat in the upper macrotidal Seine estuary, France. Estuarine, Coastal
663 and Shelf Science, 64 (4) 710-720
664
665 Deloffre, J., Lafite, R., Lesueur, P., Verney, R., Lesourd, S., Cuvilliez, A. and Taylor, J. A. (In press)
666 Controlling factors of rhythmic sedimentation processes on an intertidal estuarine mudflat - Role of
667 the maximum turbidity zone in the macrotidal Seine estuary, France. Marine Geology,
668
669 Dyer, K. R. (1994) Estuarine Sediment transport and deposition. In: Pye, K. (Eds), Sediment transport
670 and depositional processes, Blackwell Scientific Publications, 193-217
671
672 Fagerburg, T. L. and Pratt, T. C. (1998) Upper Mississippi River navigation and sedimentation field
673 data collection summary report. In: Interim Report for the upper Mississippi River - Illinois waterway
674 System navigation study, US Army Corps of Engineers (Eds), 150pp
675
676 Fredsoe, J. (1984) Turbulent boundary layer in wave-current motion. Journal of Hydraulic
677 Engineering, 110 1103-1120
678
679 Fugate, D. C. and Friedrichs, C. T. (2002) Determining concentration and fall velocity of estuarine
680 particle populations using ADV, OBS and LISST. Continental Shelf Research, 22 1867-1886
681
682 Grant, J. and Madsen, O. S. (1979) Combined wave and current interaction with a rough bottom.
683 Journal of Geophysical Research, 84 (C4) 1797-1808
684
685 Guezennec, L., Lafite, R., Dupont, J. P., Meyer, R. and Boust, D. (1999) Hydrodynamics of suspended
686 particulate matter in the tidal freshwater zone of a macrotidal estuary (the Seine estuary, France).
687 Estuaries, 22 (3A) 717-727
688

689 Huntley, D. A. (1988) A modified inertial dissipation method for estimating seabed stresses at low
690 Reynolds numbers, with application to wave/current boundary layer measurements. Journal of
691 Physical Oceanography, 18 339-346
692
693 Hutnance, J. M., Humphery, J. D., Knight, P. J., Chatwin, P. G., Thomsen, L. and White, M. (2002)
694 Near-bed turbulence measurements, stress estimates and sediment mobility at the continental shelf
695 edge. Progress in oceanography, 52 171-194
696
697 Kawanisi, K. and Yokosi, S. (1997) Characteristics of suspended sediment and turbulence in a tidal
698 boundary layer. Continental Shelf Research, 17 (8) 859-875
699
700 Kim, S.-C., Friedrichs, C. T., Maa, J. P.-Y. and Wright, L. D. (2000) Estimating bottom stress in tidal
701 boundary layer from acoustic doppler velocimeter data. Journal of Hydraulic Engineering, 126 (6)
702 399-406
703
704 Lafite, R. and Romana, L. A. (2001) A man-altered macrotidal estuary : the Seine estuary (France).
705 Estuaries, 24 (6B) 393
706
707 Le Hir, P., Roberts, W., Cazaillet, O., Christie, M. C., Bassoullet, P. and Bacher, C. (2000)
708 Characterization of intertidal flat hydrodynamics. Continental Shelf Research, 20 1433-1459
709
710 Lesourd, S. (2000) Processus d'envasement d'un estuaire macrotidal: zoom temporel du siècle à
711 l'heure; application à l'estuaire de la Seine. PhD Thesis, Université de Caen, 290pp.
712
713 Lesourd, S., Lesueur, P., Brun Cottan, J. C., Auffret, J.-P., Poupinet, N. and Laignel, B. (2001)
714 Morphosedimentary evolution of the macrotidal Seine estuary subjected to human impact. Estuaries,
715 24 (6B) 940-949
716

717 Lesourd, S., Lesueur, P., Brun-Cottan, J. C., Garnaud, S. and Poupinet, N. (2003) Seasonal variations
718 in the characteristics of superficial sediments in a macrotidal estuary (the Seine inlet, France).
719 Estuarine, Coastal and Shelf Science, 58 (1) 3-16
720
721 Mitchener, H. and Torfs, H. (1996) Erosion of mud/sand mixtures. Coastal Engineering, 29 1-25
722
723 Myrhaug, D., Slaattelid, O. H. and Lambrakos, K. F. (1998). Seabed shear stresses under random
724 waves: prediction vs estimates from field measurements. Ocean Engineering 25(10) 907-916.
725
726 O'Brien, D. J., Whitehouse, R. J. S. and Cramp, A. (2000) The cyclic development of a macrotidal
727 mudflat on varying timescales. Continental Shelf Research, 20 (12-13) 1593-1619
728
729 Parchure, T. M., McAnally, W. H. and Teeter, A. M. (2001) Wave-induced sediment resuspension
730 near the shorelines of the upper Mississippi river system. In: Interim Report for the upper Mississippi
731 River - Illinois waterway System navigation study, US Army Corps of Engineers (Eds), 31p
732
733 Sanford, L. P. and Maa, J. P.-Y. (2001) A unified erosion formulation for fine sediments. Marine
734 Geology, 179 9-23
735
736 Schoellhamer, D. H. (1996) Anthropogenic sediment resuspension mechanisms in a shallow
737 microtidal estuary. Estuarine, Coastal and Shelf Science, 43 533-548
738
739 Silva Jacinto, R. (2002) Action des vagues sur les estrans et vasières. Application à l'estuaire de Seine.
740 PhD Thesis, Université de Rouen, 231pp.
741
742 Simpson, J. H., Williams, E., Brasseur, L. H. and Brubaker, J. M. (2005) The impact of tidal straining
743 on the cycle of turbulence in a partially stratified estuary. Continental Shelf Research, 25 51-64
744

745 Soulsby, R. L. (1983) The bottom boundary layer of shelf seas. In: Johns, B. (Eds), Physical
746 oceanography of coastal and shelf seas, Elsevier, 189-266
747
748 Soulsby, R. L. (1995) Bed shear stress due to combined waves and currents. In: Stive, M. J. F., de
749 Vriend, H. J., Fredsoe, J., Hamm, L., Soulsby, R. L., Teisson, C. and Winterwerp, J. C. (Eds),
750 Advances in coastal moprhodynamics, Delft Hydraulics, 4:20-4:23
751
752 Soulsby, R. L. (1997) Dynamics of marine sands. A manual for practical applications. Thomas
753 Telford, London,249p.
754
755 Soulsby, R. L., Hamm, L., Klopman, G., Myrhaug, D., Simons, R. R. and Thomas, G. P. (1993)
756 Wave-current interaction within and outside the bottom boundary layer. Coastal Engineering, 21 41-69
757
758 Soulsby, R. L. and Humphery, J. D. (1990) Field observations of wave-current interaction at the sea
759 bed. In: Torum, A. and Gudmestad, O. T. (Eds), Water wave kinematics, Kluwer Academic
760 Publishers, 413-428
761
762 Talke, S. A. and Stacey, M. T. (2003) The influence of oceanic swell on flows over an estuarine
763 intertidal mudflat in San Francisco Bay. Estuarine, Coastal and Shelf Science, 58 541-554
764
765 Thorne, P. D. and Hanes, D. M. (2002) A review of acoustic measurements of small-scale sediment
766 processes. Continental Shelf Research, 22 603-632
767
768 Tolhurst, T. J., Black, K. S., Paterson, D. M., Mitchener, H. J., Termaat, G. R. and Shayler, S. A.
769 (2000) A comparison and measurement standardisation of four in situ devices for determining the
770 erosion shear stress of intertidal sediments. Continental Shelf Research, 20 1397-1418
771

772 Trembanis, A. C., Wright, L. D., Friedrichs, C. T., Green, M. O. and Hume, T. (2004) The effects of
773 spatially complex inner shelf roughness on boundary layer turbulence and current and wave friction:
774 Tairua embayment, New Zealand. Continental Shelf Research, 24 (13-14) 1549-1571
775
776 Uncles, R. J., Easton, A. E., Griffiths, M. L., Harris, C. K., Howland, R. J. M., King, R. S., Morris, A.
777 W. and Plummer, D. H. (1998) Seasonality of the turbidity maximum in the Humber-Ouse Estuary,
778 UK. Marine Pollution Bulletin, 37 (3-7) 206-215
779
780 Verney, R., Brun Cottan, J. C., Lafite, R., Deloffre, J. and Taylor, J. A. (2006) Tidal-induced shear
781 stress variability above intertidal mudflats. Case of the macrotidal Seine estuary. Estuaries, 29 (4) 653-
782 664
783
784 Voulgaris, G. and Meyers, S. T. (2004) Temporal variability of hydrodynamics, sediment
785 concentration and sediment settling velocity in a tidal creek. Continental Shelf Research, 24 (15)
786 1659-1683
787
788 Voulgaris, G. and Trowbridge, J. H. (1998) Evaluation of the acoustic doppler velocimeter (ADV) for
789 turbulence measurements. Journal of Atmospheric and Oceanic Technology, 15 272-289
790
791 Williams, J. J., Rose, C. P., Thorne, P. D., O'Connor, B. A., Humphery, J. D., Hardcastle, P. J.,
792 Moores, S. P., Cooke, J. A. and Wilson, D. J. (1999) Field observations and predictions of bed shear
793 stresses and vertical suspended sediment concentration profiles in wave-current conditions.
794 Continental Shelf Research, 19 507-536
795
796 Winterwerp, J. C. and van Kesteren, W. G. M. (2004) Introduction to the physics of cohesive sediment
797 in the marine environment. Elsevier, Amsterdam, 558pp.

9. Figure Caption

Table I: Summary of hydrodynamic features (Significant wave height and maximum velocity fluctuations), suspended particulate matter concentration and bed elevation measurements during boat passages above the Oissel intertidal mudflat. (H_S LW: significant long-wave height; H_S SW: significant short-wave height; ΔU LW : long-wave-induced velocity fluctuation; ΔU SW : short-wave-induced velocity fluctuation)

Fig. 1: The Seine estuary and study sites: The Oissel Mudflat (kp 230) in the upper estuary and the Vasière Nord mudflat (kp 355) at the estuary mouth. Position of the instrumented MAREL Buoy. (Kilometric point (kp): distance from the Pont Marie, Paris) (Channel width exaggerated upstream kp 350 to clarify the figure)

Fig. 2: Calibration of the 6 MHz Nortek ADV backscattered amplitude with weighted suspended sediment concentration: experimental results (this study) and data from Voulgaris and Meyer (2004) from a 10 MHz Sontek ADV

Fig. 3: Hydrodynamic features during a W-SW 8 m s^{-1} wind event above the Vasière Nord intertidal mudflat: (a) instantaneous wave height; (b) significant wave height (H_S) and period (T) over a one minute period; (c) TKE shear stress (τ_{TKE}), and Wave-Current shear stress (τ_{WC}) for a bed roughness length of 0.37 mm. The shadow area shows the τ_{WC} variability as a function of low (0.2mm) or large (0.7mm) bed roughness length

Fig. 4: Boat passages above the Oissel intertidal mudflat: (a) Wave height during the tidal cycle and zoom on one boat passage: (b) wave height (c) and 3D current velocity variations.

Fig. 5: Typical hydrodynamic signature of a boat passage above the Oissel intertidal mudflat : (a) wave height ; (b) long wave height and (c) short wave height; (d) short waves ($\tau_{W\text{-}SW}$), long waves ($\tau_{W\text{-}LW}$) and combined short-long waves ($\tau_{W\text{-}LW+SW}$) shear stresses and (e) bottom shear stress calculations : combined short-long waves ($\tau_{W\text{-}LW+SW}$) shear stress, wave-current shear stress (τ_{WC}) and TKE shear stress (τ_{TKE})

Fig. 6: Impact of boat passages on hydrodynamic features above the Oissel mudflat during a tidal cycle: (a) mean water level and mean current velocity (U) and (b) wave-current shear stress (τ_{WC}) and TKE shear stress (τ_{TKE}).

Fig. 7: Variability of hydrodynamic and sedimentary parameters during high spring tides above the Vasière Nord mudflat. (a) water level; (b) wind speed and direction measured at the MAREL Buoy; (c) significant wave height (H_S); (d) wave-current shear stress (τ_{WC}); (e) SPM concentration (C_{SPM}) and (f) bed elevation variations. Sedimentation periods are indicated by grey dots and the erosion periods by black dots

Fig. 8: Variability of the bed roughness length during a fortnightly survey at the Oissel Mudflat.

Fig. 9: Variability of hydrodynamic and sedimentary parameters during a semi-lunar cycle above the Oissel mudflat. (a) water level; (b) wave-current shear stress (τ_{WC}); (c) SPM concentration (C_{SPM}) and (d) bed elevation variations

Figure 10: Comparison between bottom shear stress (τ_{WC}) and SPM concentration (C_{SPM}) values above the Oissel Mudflat: determination of the critical erosion shear stress

Figure Caption

Table I: Summary of hydrodynamic features (Significant wave height and maximum velocity fluctuations), Suspended Particulate Matter concentration and bed elevation measurements during boat passages above the Oissel intertidal mudflat. (H_S LW: significant long-wave height; H_S SW : significant short-wave height; ΔU LW : long-wave-induced velocity fluctuation; ΔU SW : short-wave-induced velocity fluctuation)

Fig. 1: The Seine estuary and sites studied: The Oissel Mudflat (kp 230) in the upper estuary and the Vasière Nord mudflat (kp 355) at the estuary mouth. Position of the instrumented MAREL Buoy. (Kilometric point (kp): distance from the Pont Marie, Paris) (Channel width exaggerated upstream kp 350 to clarify the figure)

Fig. 2: Calibration of the 6 MHz Nortek ADV backscattered amplitude with weighted suspended sediment concentration : experimental results (this study) and data from Voulgaris and Meyer (2004) from a 10 MHz Sontek ADV

Fig. 3: Hydrodynamic features during a W-SW 8 m s^{-1} wind event above the Vasière Nord intertidal mudflat: (a) instantaneous wave height; (b) significant wave height (H_S) and period (T) over a one minute period; (c) TKE shear stress (τ_{TKE}), and Wave-Current shear stress (τ_{WC}) for a bed roughness length of 0.37 mm. The shadow area shows the τ_{WC} variability as a function of low (0.2mm) or large (0.7mm) bed roughness length

Fig. 4: Boat passages above the Oissel intertidal mudflat: (a) Wave height during the tidal cycle and zoom on one boat passage : (b) wave height (c) and 3D current velocity variations.

Fig. 5: Typical hydrodynamic signature of a boat passage above the Oissel intertidal mudflat : (a) wave height ; (b) long wave height and (c) short wave height; (d) short waves ($\tau_{W\text{-}SW}$), long waves ($\tau_{W\text{-}LW}$) and combined short-long waves ($\tau_{W\text{-}LW+SW}$) shear stresses and (e) bottom shear stress calculations : combined short-long waves ($\tau_{W\text{-}LW+SW}$) shear stress, wave-current shear stress (τ_{WC}) and TKE shear stress (τ_{TKE})

Fig. 6: Impact of boat passages on hydrodynamic features above the Oissel mudflat during a tidal cycle: (a) mean water level and mean current velocity (U) and (b) Wave-current shear stress (τ_{WC}) and TKE shear stress (τ_{TKE}).

Fig. 7: Variability of hydrodynamic and sedimentary parameters during high spring tides above the Vasière Nord mudflat. (a) water level; (b) wind speed and direction measured at the MAREL Buoy; (c) significant wave height (H_S); (d) wave-current shear stress (τ_{WC}); (e) SPM concentration (C_{SPM}) and (f) bed elevation variations. Sedimentation periods are indicated by grey dots and the erosion periods by black dots

Fig. 8: Variability of the bed roughness length during a fortnightly survey at the Oissel Mudflat.

Fig. 9: Variability of hydrodynamic and sedimentary parameters during a semi-lunar cycle above the Oissel mudflat. (a) water level; (b) wave-current shear stress (τ_{WC}); (c) SPM concentration (C_{SPM}) and (d) bed elevation variations

Figure 10: Comparison between bottom shear stress (τ_{WC}) and SPM concentration (C_{SPM}) values above the Oissel Mudflat: determination of the critical erosion shear stress

Table I

Boat Nb	Water height above the bed (m)	Hs LW (m)	Hs SW (m)	◊U LW (m s^{-1})	◊U SW (m s^{-1})	Resuspension (mg l^{-1})	Erosion (mm)
1	0.7	0.1	0.15	0.15	0.2	500	NO
2	0.35	-	-	0.15	0	100	NO
3	0.35	0.1	0.08	0.05	0.15	100	NO
4	0.5	0.05	0	0.1	0	0	NO
5	0.55	0.2	0.05	0.5	0.1	500	NO
6	0.3	-	-	0.1	0	0	NO
7	0.4	-	-	0.1	0.2	450	NO
8	1.4	0.05	0.05	0.1	0.05	50	NO
9	0.5	0.05	0	0.1	0	0	NO
10	0.2	-	-	0.3	0.2	1500	6

Figure 1

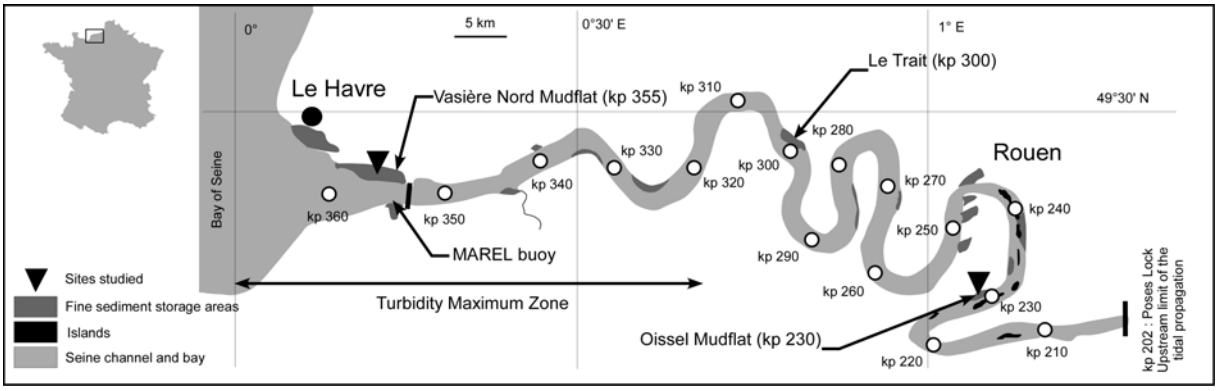
0°
5 km
0°30' E
1° E
49°30' N
Le Havre
Vasière Nord Mudflat (kp 355)
Le Trait (kp 300)
Rouen
Bay of Seine
kp 360
kp 350
kp 340
kp 330
kp 320
kp 310
kp 300
kp 290
kp 280
kp 270
kp 260
kp 250
kp 240
kp 230
kp 220
kp 210
MAREL buoy
Turbidity Maximum Zone
Oissel Mudflat (kp 230)
kp 202 : Poses Lock
Upstream limit of the
tidal propagation
Sites studied
Fine sediment storage areas
Islands
Seine channel and bay

Figure 2

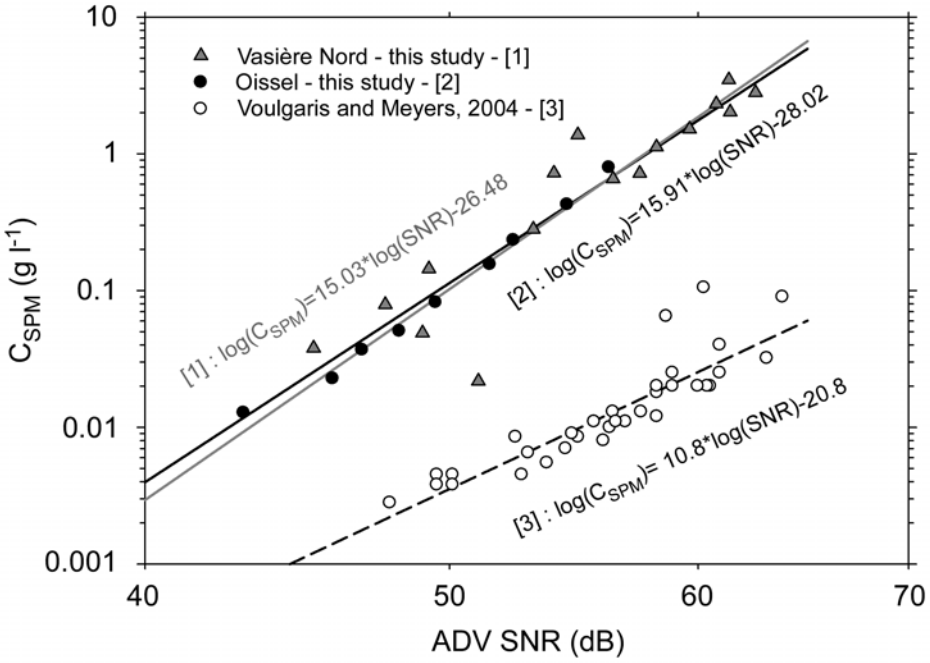
Vasière Nord - this study - [1]
Oissel - this study - [2]
Voulgaris and Meyers, 2004 - [3]
[1] : log(C_SPM)=15.03*log(SNR)-26.48
[2] : log(C_SPM)=15.91*log(SNR)-28.02
[3] : log(C_SPM)= 10.8*log(SNR)-20.8
C_SPM (g l^-1)
ADV SNR (dB)
10
1
0.1
0.01
0.001
40
50
60
70

Figure 3

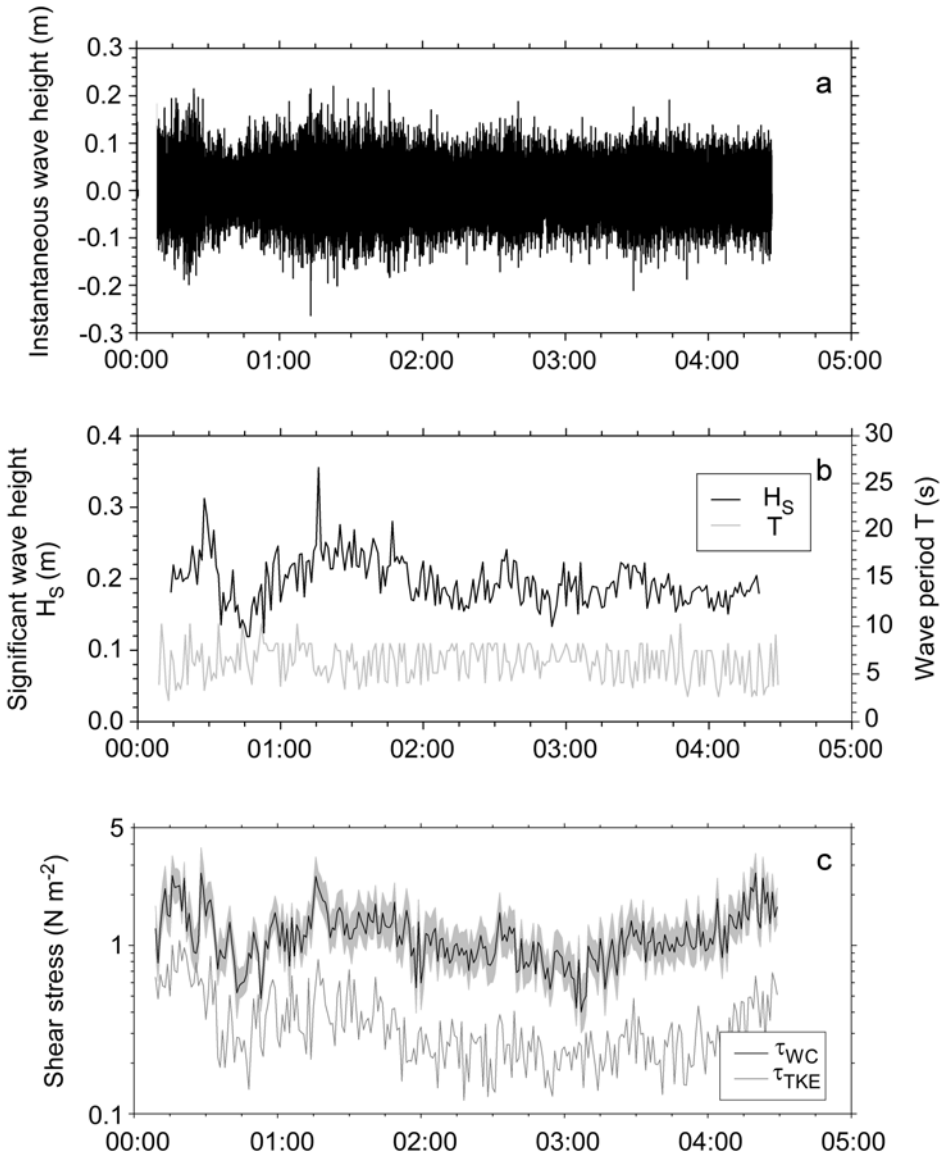
Instantaneous wave height (m)
0.3
0.2
0.1
0.0
-0.1
-0.2
-0.3
a
00:00
01:00
02:00
03:00
04:00
05:00
Significant wave height
H_S (m)
0.4
0.3
0.2
0.1
0.0
b
H_S
T
30
25
20
15
10
5
0
Wave period T (s)
00:00
01:00
02:00
03:00
04:00
05:00
Shear stress (N m^{-2})
5
1
0.1
c
τ_{WC}
τ_{TKE}
00:00
01:00
02:00
03:00
04:00
05:00

Figure 4

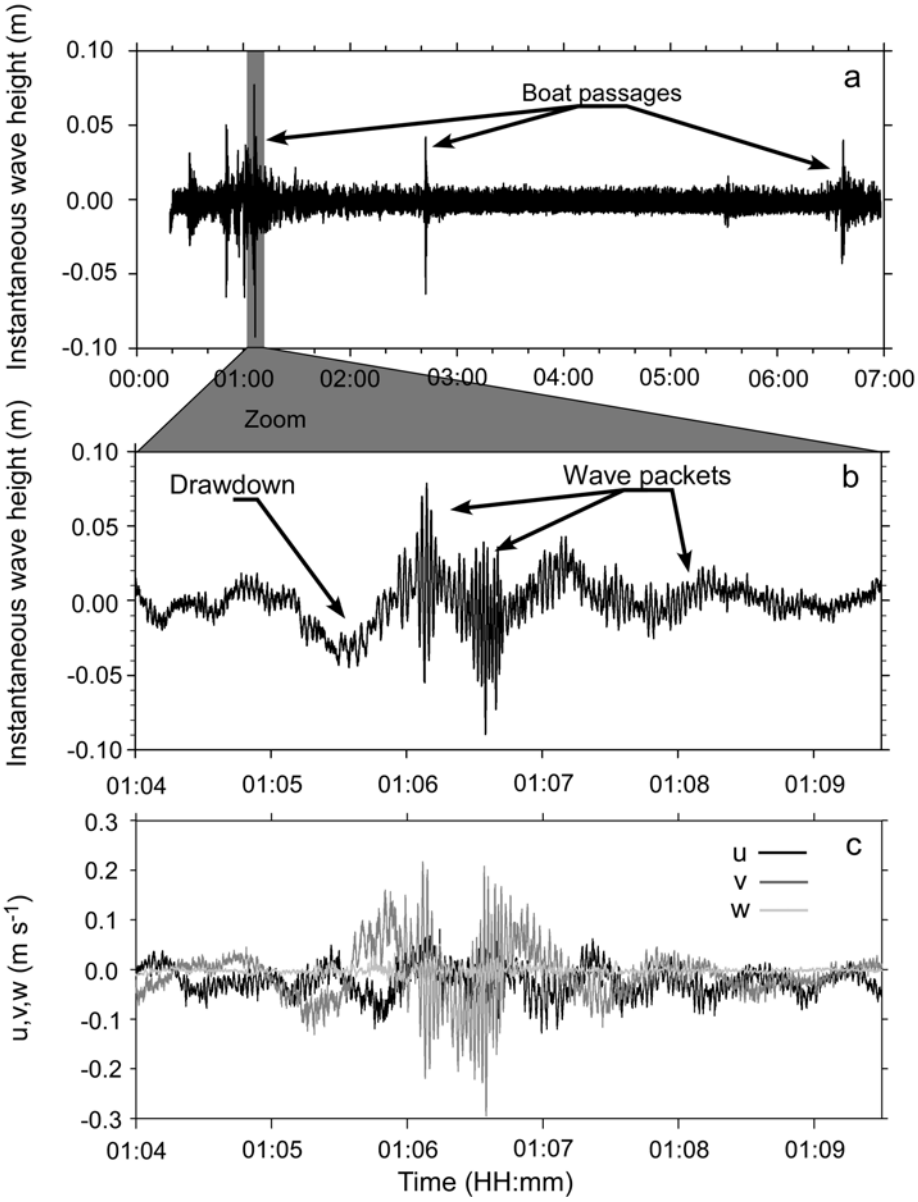
Instantaneous wave height (m)
0.10
0.05
0.00
-0.05
-0.10
a
Boat passages
00:00
01:00
02:00
03:00
04:00
05:00
06:00
07:00
Zoom
Instantaneous wave height (m)
Drawdown
Wave packets
b
01:04
01:05
01:06
01:07
01:08
01:09
u,v,w (m s-1)
0.3
0.2
0.1
0.0
-0.1
-0.2
-0.3
u
v
w
c
Time (HH:mm)

Figure 5

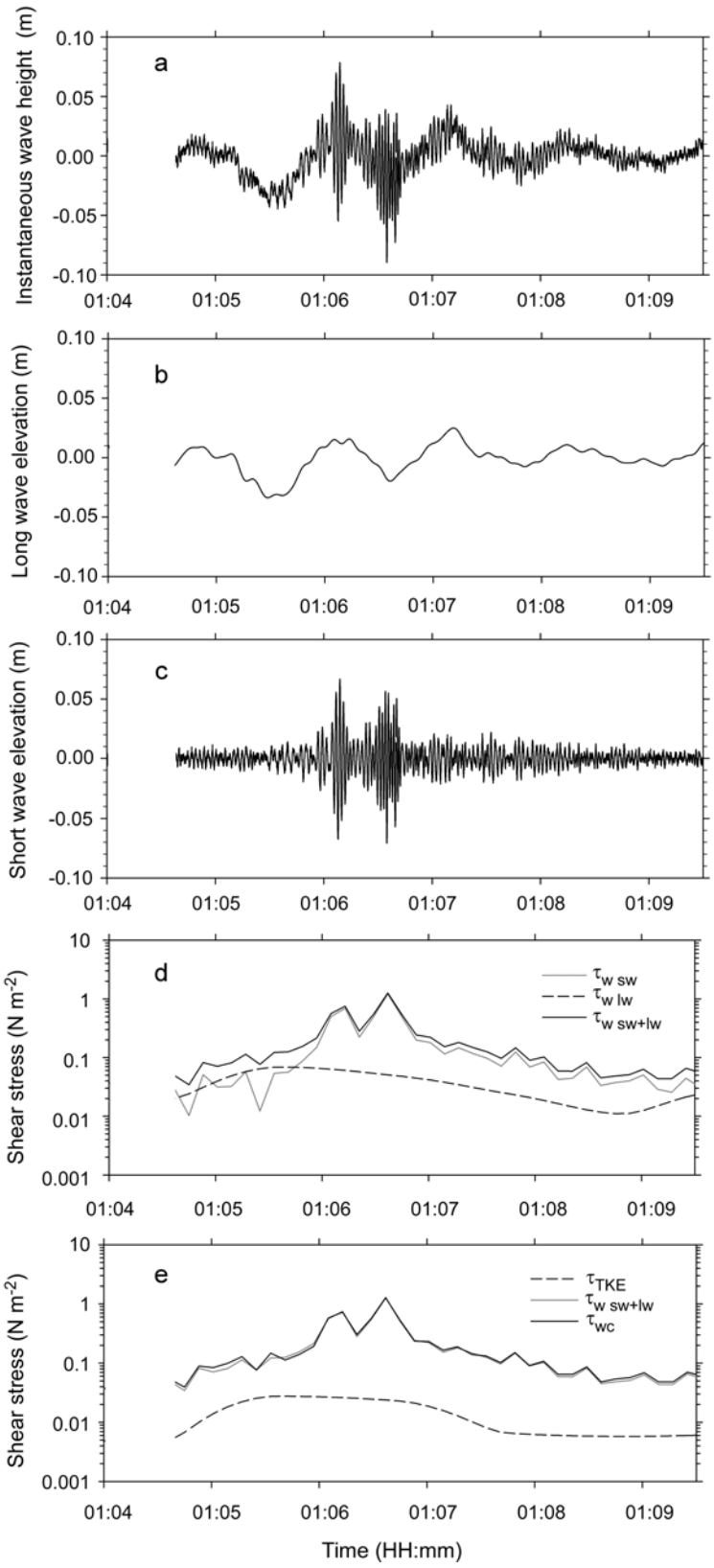
a
b
c
d
e
Instantaneous wave height (m)
Long wave elevation (m)
Short wave elevation (m)
Shear stress (N m-2)
Shear stress (N m-2)
0.10
0.05
0.00
-0.05
-0.10
10
1
0.1
0.01
0.001
01:04
01:05
01:06
01:07
01:08
01:09
τw sw
τw lw
τw sw+lw
τTKE
τw sw+lw
τwc
Time (HH:mm)

Figure 6

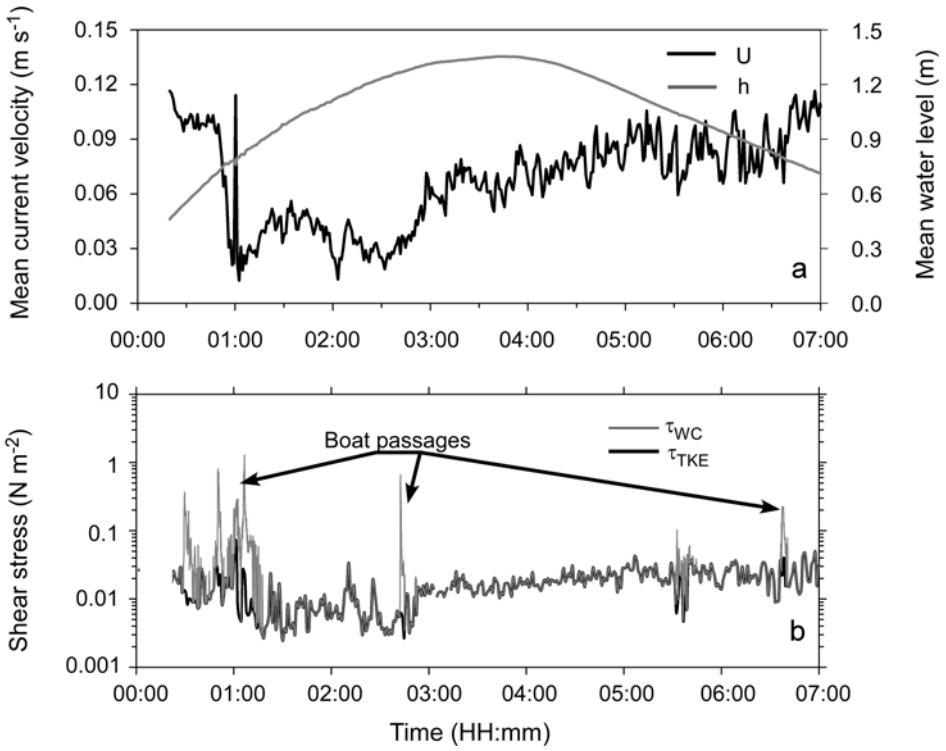
Mean current velocity (m s-1)
Mean water level (m)
U
h
a
Boat passages
τWC
τTKE
b
Shear stress (N m-2)
Time (HH:mm)
00:00
01:00
02:00
03:00
04:00
05:00
06:00
07:00

Figure 7

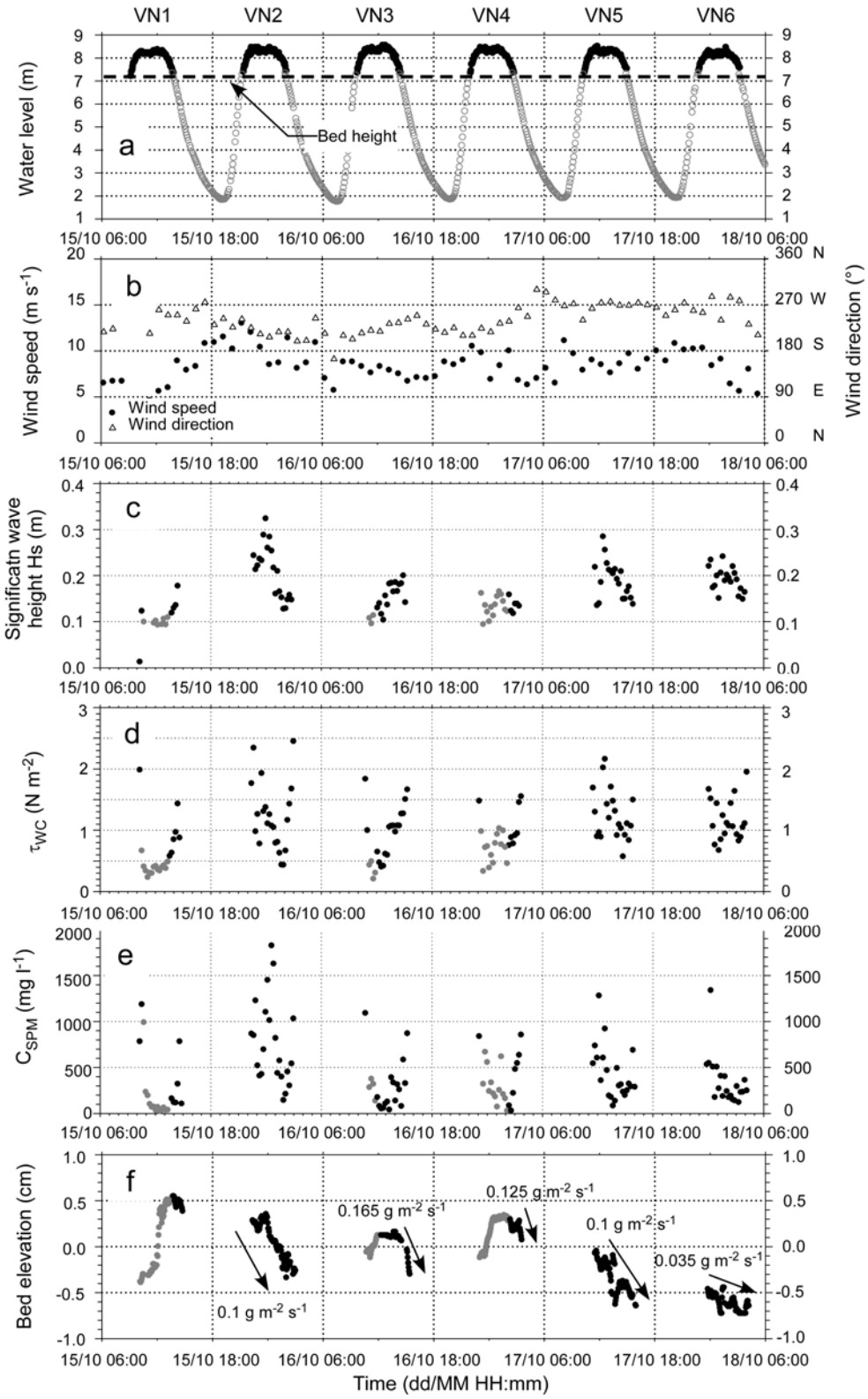
VN1
VN2
VN3
VN4
VN5
VN6
Water level (m)
Bed height
a
15/10 06:00
15/10 18:00
16/10 06:00
16/10 18:00
17/10 06:00
17/10 18:00
18/10 06:00
Wind speed (m s-1)
Wind direction (°)
b
Wind speed
Wind direction
360 N
270 W
180 S
90 E
0 N
Significatn wave height Hs (m)
c
τWC (N m-2)
d
CSPM (mg l-1)
e
Bed elevation (cm)
f
0.1 g m-2 s-1
0.165 g m-2 s-1
0.125 g m-2 s-1
0.1 g m-2 s-1
0.035 g m-2 s-1
Time (dd/MM HH:mm)

Figure 8

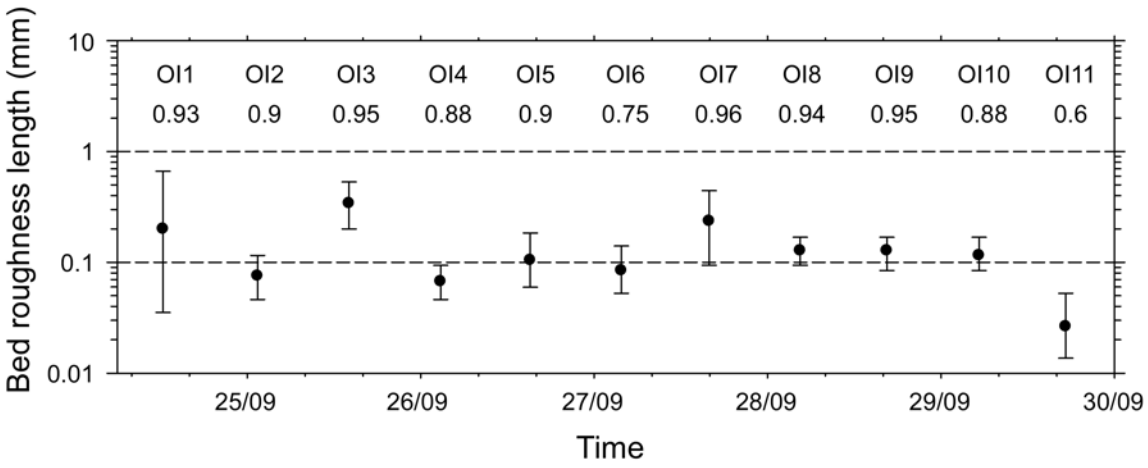
Bed roughness length (mm)
10
1
0.1
0.01
OI1 OI2 OI3 OI4 OI5 OI6 OI7 OI8 OI9 OI10 OI11
0.93 0.9 0.95 0.88 0.9 0.75 0.96 0.94 0.95 0.88 0.6
25/09
26/09
27/09
28/09
29/09
30/09
Time

Figure 9

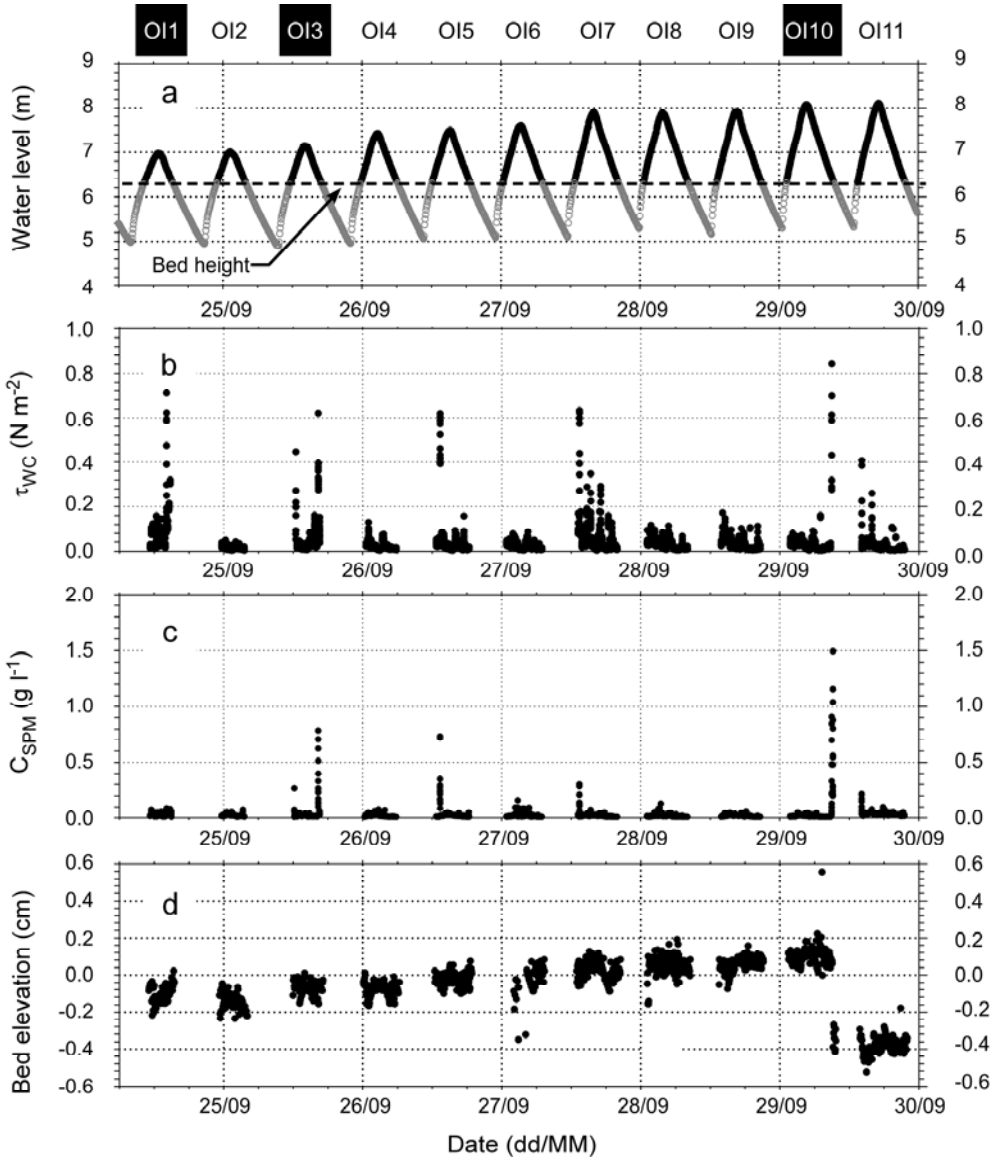
OI1
OI2
OI3
OI4
OI5
OI6
OI7
OI8
OI9
OI10
OI11
a
Water level (m)
Bed height
b
τ_{WC} (N m^{-2})
c
C_{SPM} (g l^{-1})
d
Bed elevation (cm)
25/09
26/09
27/09
28/09
29/09
30/09
Date (dd/MM)

Figure 10

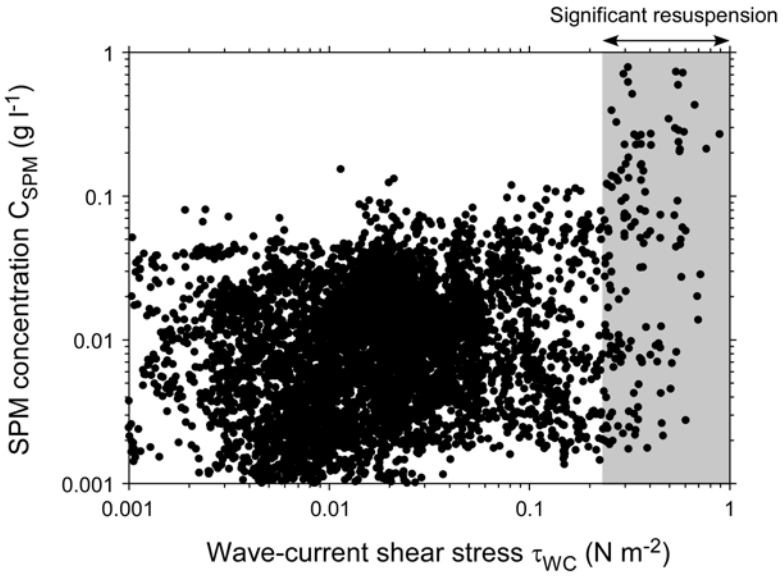
Significant resuspension
SPM concentration C_{SPM} (g l^{-1})
1
0.1
0.01
0.001
0.001
0.01
0.1
1
Wave-current shear stress τ_{WC} (N m^{-2})